CONF-800104--7

HEAT TRANSFER INCLUDING PARTICLE AND GAS RADIATION IN SUBSONIC MHD DIFFUSER-II

by

R. K. Ahluwalia and Kwan H. Im

MASTER

Prepared for

AIAA 18th Aerospace Sciences Meeting

Pasadena, California

January 14-16, 1980

U of C-AUA-USDOE

ARGONNE NATIONAL LABORATORY, ARGONNE, ILLINOIS

Operated under Contract W-31-109-Eng-38 for the

U. S. DEPARTMENT OF ENERGY

The facilities of Argonne National Laboratory are owned by the United States Government. Under the terms of a contract (W-31-109-Eng-38) among the U. S. Department of Energy, Argonne Universities Association and The University of Chicago, the University employs the staff and operates the Laboratory in accordance with policies and programs formulated, approved and reviewed by the Association.

MEMBERS OF ARGONNE UNIVERSITIES ASSOCIATION

The University of Arizona
Carnegie-Mellon University
Case Western Reserve University
The University of Chicago
University of Cincinnati
Illinois Institute of Technology
University of Illinois
Indiana University
The University of Iowa
Iowa State University
The University of Kansas
Kansas State University
Loyola University of Chicago
Marquette University
The University of Michigan
Michigan State University
University of Minnesota
University of Missouri
Northwestern University
University of Notre Dame
The Ohio State University
Ohio University
The Pennsylvania State University
Purdue University
Saint Louis University
Southern Illinois University
The University of Texas at Austin
Washington University
Wayne State University
The University of Wisconsin-Madison

HEAT TRANSFER INCLUDING PARTICLE AND GAS RADIATION IN SUBSONIC MHD DIFFUSER-II*

R. K. Ahluwalia and Kwan H. Im
Argonne National Laboratory
Argonne, Illinois 60439

Abstract

Heat transfer in subsonic MHD diffusers, by convection and by gas and slag particle radiation, is analyzed by simultaneously solving the radiation transport equation and the quasi-three-dimensional gasdynamic equations. The efficiency factors for extinction and scattering by particles are calculated from the Mie theory. For a reference diffuser geometry, the heat transfer by convection is found to be 25 MW, and the radiative heat transfer varies from 44 MW to 79 MW, depending on the rate of ash carryover into the channel. Results reveal that the heat transfer is sensitive to the ash carryover into the channel, slag particles spectrum, electrical conductivity of ash, gas composition, and wall emissivity. It is observed that, because of multiple scattering, the particles shield the short wavelength radiation emitted by potassium atoms. The impacts of heat transfer enhancement by gas radiation in the channel and by gas-plus-particles radiation in the diffuser on MHD system design are assessed. It is suggested that, from the system design point of view, the diffuser be regarded as a part of the radiant boiler. No significant effect of radiation enhancement on the ability to decompose NO_x is anticipated.

Nomenclature

$\bar{A}$	cross-sectional area
A, B	parameters in mixing length model
a_ν, b_ν	parameters defined in Eqs. (13) and (17)
a_ℓ, b_ℓ	Mie complex scattering coefficients
C_p	pressure recovery coefficient
h, h_c	enthalpy and its value at center line
I_ν, $I_{b\nu}$ $I_{w\nu}$	radiation intensity, and Planck functions at gas temperature and at surface temperature
G_ν	incident radiation
k_s, k_s^+	wall roughness and its non-dimensional quantity
m	complex refractive index
n, N	particle-size distribution function and number density
N_o, $\langle r\rangle_o$	number density and average size at diffuser inlet
p	pressure
$\dot{q}_r$, $\dot{q}_{rs}$ $\dot{q}_{r\nu}$	radiative heat flux, its wall value and its spectral value
r	particle radius
S_ν	scattering function
u, u_c $\langle u\rangle$	axial component of gas velocity, its centerline value, and its average value
u_τ	shear velocity
v	normal component of gas velocity
W	channel width
x, y, z	Cartesian coordinates
α_ν	parameter defined in Eq. (21)
β_ν, ω_ν	extinction coefficient and scattering albedo
τ, τ_o	optical thickness and its value at wall
τ_{xy}, τ_s	shear stress and its value at wall
ρ, ρ_c	gas density and its value at centerline
μ_{eff}	effective viscosity
μ	cosine of the cone angle
ε_w	wall emissivity
ε_m, ε_h	turbulent momentum and enthalpy diffusivities
ν_w	molecular diffusivity at wall temperature
δ_1, δ_2, δ_3	displacement, momentum, and enthalpy thicknesses
δ	boundary layer thickness
$\chi_{e\nu}$, $\chi_{s\nu}$	efficiency factors for extinction and scattering
λ	wavelength (μm)
θ	divergence half angle of diffuser
σ_e	electrical conductivity of slag(S)

I. Introduction

The performance of MHD diffusers is closely tied to the state of the plasma exiting the channel. The channel exit conditions depend in general on the channel size and operating conditions. However, for base-load applications, three important flow-related events will invariably have taken place in the channel before the plasma reaches the diffuser. First, the flow will become almost fully-developed. Second, the slag vapors will, for all practical purposes, be depleted. Third, nucleation of new

particles or growth of particles formed in the channel will be precluded in the diffuser because no slag vapors are available. Therefore, the particle size and number will remain constant throughout the diffuser if changes resulting from possible agglomeration of particles and slag deposition on diffuser walls are neglected.

Because of the thick boundary layer, heat transfer by convection and radiation will be of the same order throughout the diffuser. The additional complication is that, because of their comparatively high number density, the slag particles of submicrometer size begin to play an important role in promoting radiative heat transfer. In fact, the heat transfer by particles may exceed that by gas alone by a factor of two, or even three. This is why it was so crucial in Part I (see Ref. 1) to trace as closely as possible the history of the particles formed in the channel.

In the past, Doss[2] and Roy[3] have analyzed the performance of MHD diffusers with high blockages. Neither of the two studies recognizes the sizeable contributions of gas and particle radiation to heat transfer. At the very outset, the present work serves to remove this limitation in the formulations of Refs. 2 and 3. The present work also employs a more accurate quasi-three-dimensional gasdynamic model, which is coupled to the radiation transport equation. The possibility of radiation scattering by slag particles is included in the radiation transport equation. The efficiency factors for extinction and scattering (caused by particles) are evaluated directly from the Mie theory.[4] The absorption coefficients for carbon dioxide and water vapor are computed from the exponential wide band model,[5] and for potassium atoms from certain correlations of experimental data.[6] A closed-form solution of the radiation transport equation is first obtained by invoking the P_1 approximation.[7] The complete diffuser model equations are then solved numerically.

Various diffuser calculations are performed for entrance conditions complementing the channel exit conditions of Ref. 1. The slag particle size spectra enumerated in Ref. 1 are employed in the form of histograms in these calculations. It is found that, for the reference diffuser geometry adopted, heat transfer by convection is 25 MW, and the radiative heat transfer varies from 44 MW for 8% ash carryover to 79 MW for 100% ash carryover into the channel.

The impacts of heat transfer enhancement by gas radiation in the channel and gas-plus-particles radiation in the diffuser on system design and on NO_x decomposition have been assessed, It is recommended that, for system design considerations, the diffuser be regarded as part of the radiant boiler.

II. Diffuser Model and Analysis

The governing equations are comprised of quasi-three-dimensional gasdynamic equations, an equation to ensure slag particles number conservation, and a radiation transport equation. The particle number conservation equation is linked to gasdynamics through the average flow velocity. The radiation transport equation supplies the divergence of radiant heat flux and wall heat flux to the energy equation, but is itself coupled to gasdynamics through the temperature profile. The gasdynamic equations listed below are essentially the same as those presented in Ref. 1, except for the absence of the magnetohydrodynamic terms. The radiation transport equation, Eq. (6), contains a term to account for the scattering of radiation by slag particles.

Continuity

$$\frac{\partial}{\partial x}\left[\rho u(W-2\delta_{1s})\right] + \frac{\partial}{\partial y}\left[\rho v(W-2\delta_{1s})\right] = 0 \qquad (1)$$

x-Momentum

$$\frac{\partial}{\partial x}\left[\rho uu(W-2\delta_{2s})\right] + \frac{\partial}{\partial y}\left[\rho uv(W-2\delta_{2s})\right] = -W\frac{\partial p}{\partial x} + W\frac{\partial}{\partial y}\left(\mu_{eff}\frac{\partial u}{\partial y}\right) - 2\tau_s \qquad (2)$$

y-Momentum

$$\frac{\partial p}{\partial y} = 0 \qquad (3)$$

Total Energy

$$\frac{\partial}{\partial x}\left[\rho u\left(h+\tfrac{1}{2}u^2\right)(W-2\delta_{3s})\right] + \frac{\partial}{\partial y}\left[\rho v\left(h+\tfrac{1}{2}u^2\right)(W-2\delta_{3s})\right] = W\frac{\partial}{\partial y}\left(k_{eff}\frac{\partial h}{\partial y}\right) + W\frac{\partial \dot{q}_r}{\partial y} + W\frac{\partial}{\partial y}\left(u\,\tau_{xy}\right) - 2\left(\dot{q}_c + \dot{q}_{rs}\right) \qquad (4)$$

where δ_1, δ_2, and δ_3 are, in that order, the displacement, momentum, and enthalpy thicknesses, defined for convenience as,

$$\delta_{1s} = \int_0^{\delta_s}\left(1 - \frac{\rho u}{\rho_c u_c}\right)dz$$

$$\delta_{2s} = \int_0^{\delta_s}\left(1 - \frac{\rho u^2}{\rho_c u_c^2}\right)dz$$

$$\delta_{3s} = \int_0^{\delta_s}\left[1 - \frac{\rho u\left(h+\frac{1}{2}u^2\right)}{\rho_c u_c\left(h_c+\frac{1}{2}u_c^2\right)}\right]dz$$

In the foregoing equation, the subscript s refers to the sidewalls.

Slag Number Conservation

$$\frac{d}{dx}\left(N \bar{A} \langle u \rangle\right) = 0 \tag{5}$$

Radiation Transport Equation

$$\mu \frac{\partial I_\nu}{\partial y} + \beta_\nu I_\nu (y,\mu) = (1-\omega_\nu)\beta_\nu I_{b\nu} + \frac{1}{2}\omega_\nu\beta_\nu \int_{-1}^{1} S_\nu(\mu,\mu') I_\nu(y,\mu')\, d\mu' \tag{6}$$

Analytical Solution of Radiation Transport Equation

The gradient of radiant heat flux can be obtained by integrating Eq. (6) with respect to μ and ν

$$\frac{d\dot{q}_r}{dy} = 4\pi \int_0^\infty (1-\omega_\nu)\,\beta_\nu \left(I_{b\nu} - \frac{G_\nu}{4\pi}\right) d\nu \tag{7}$$

where G_ν, the incident radiation, may be evaluated by integrating the spectral radiation intensity (I_ν) as

$$G_\nu(y) = 2\pi \int_{-1}^{1} I_\nu(y,\mu)\, d\mu \tag{8}$$

and

$$\dot{q}_r = 2\pi \int_0^\infty d\nu \int_{-1}^{1} \mu\, I_\nu(y,\mu)\, d\mu$$

In order to solve Eq. (6), I_ν and S_ν are expanded in terms of Legendre polynomials and substituted into Eq. (6), to obtain the following equations for $\dot{q}_{r\nu}$ and G_ν.

$$\frac{d\dot{q}_{r\nu}}{d\tau} + (1-\omega_\nu)\, G_\nu = 4\pi\,(1-\omega_\nu)\, I_{b\nu} \tag{9}$$

$$\frac{dG_\nu}{d\tau} + 3\,\dot{q}_{r\nu} = 0 \tag{10}$$

where

$$\tau = \int_0^y \beta_\nu(y')\, dy'$$

In writing Eq. (10), a nonessential assumption has been made, namely, the scattering function is an isotropic one. Employing the P_1 approximation[7], in which only the zero and first-order terms are retained, one has

$$I_\nu(\tau,\mu) = \frac{1}{4\pi} G_\nu(\tau) + \frac{3}{4\pi}\dot{q}_{r\nu}(\tau)\,\mu \tag{11}$$

Equations (9) and (10) can be combined into a single equation:

$$\frac{d^2 G_\nu}{d\tau^2} - a_\nu^2 G_\nu = -4\pi a_\nu^2 I_{b\nu} \tag{12}$$

where

$$a_\nu = \sqrt{3\,(1-\omega_\nu)} \tag{13}$$

The centerline symmetry condition and the boundary condition for specularly reflecting walls are:

$$I_\nu(0,-\mu) = I_\nu(0,\mu), \quad \mu > 0 \tag{14}$$

$$I_\nu(\tau_0,-\mu) = \varepsilon_W I_{b\nu}(T_W) + (1-\varepsilon_W)\, I_\nu(\tau_0,\mu), \quad \mu > 0 \tag{15}$$

Using Mark's boundary condition,[8] μ in Eq. (11) is replaced by $\mu_0 (=\sqrt{1/3})$. This is the value of μ that makes the second-order solution identically equal to zero. Using Eq. (11), the two boundary conditions can be rewritten as

$$\left(\frac{dG_\nu}{d\tau}\right)_0 = 0, \text{ and}$$

$$G_\nu(\tau_0) + b_\nu \left(\frac{dG_\nu}{d\tau}\right)_0 = 4\pi\, I_{W\nu} \tag{16}$$

where

$$b_\nu = \frac{1}{\sqrt{3}}\left(\frac{2-\varepsilon_W}{\varepsilon_W}\right) \tag{17}$$

Using the Green function approach and assuming a_ν to be a slowly varying function, the following solution for G_ν may be constructed.

$$G_\nu = 4\pi I_{W\nu} + 4\pi \int_0^{\tau_0} K_\nu(\tau|\xi)\, a_\nu^2 (I_{b\nu} - I_{W\nu})\, d\xi \tag{18}$$

with

$$K_\nu(\tau|\xi) = \frac{\left(e^{a_\nu\xi} + e^{-a_\nu\xi}\right)}{2(1-\alpha_\nu)\, a_\nu}\left(\alpha_\nu e^{a_\nu\tau} + e^{-a_\nu\tau}\right) \quad \text{when } \tau > \xi \tag{19}$$

and

$$K_\nu(\tau|\xi) = \frac{\alpha_\nu e^{a_\nu \xi} + e^{-a_\nu \xi}}{2(1-\alpha_\nu)\, a_\nu} \left(e^{a_\nu \tau} + e^{-a_\nu \tau}\right)$$

when $\tau < \xi$ (20)

where

$$\alpha_\nu = \frac{b_\nu a_\nu - 1}{b_\nu a_\nu + 1}\, e^{-2a_\nu \tau_o} \quad (21)$$

This completes the solution.

Radiation Properties

Carbon dioxide, water vapor, and potassium atoms are considered to be the principal participating gases. The spectral absorption coefficients for carbon dioxide and water vapor are evaluated from the exponential wideband model.[5] For atomic potassium, effective absorption for potassium occurs in the range $7465 < \lambda(A°) < 8199$ and is given by the correlation presented in the preceding paper (see Ref. 1).

The Mie theory[4] is employed to calculate the scattering and absorption coefficients for slag particles. Without going into lengthy details, the following are the efficiency factors for extinction and scattering:

$$\chi_{e\nu} = 2\left(\frac{\lambda}{2\pi r}\right)^2 \sum_{\ell=0}^{\infty} (2\ell+1)\, \mathrm{Re}(a_\ell + b_\ell) \quad (22)$$

$$\chi_{s\nu} = 2\left(\frac{\lambda}{2\pi r}\right)^2 \sum_{\ell=0}^{\infty} (2\ell+1)\left(|a_\ell|^2 + |b_\ell|^2\right) \quad (23)$$

where the coefficients, a_ℓ and b_ℓ, are complex numbers. These coefficients are functions of two parameters, $\frac{2\pi r}{\lambda}$ and m, the complex refractive index.

For a medium containing particles of many sizes, the overall extinction coefficient, gas-plus-particles, and scattering albedo are determined by the following equations:

$$\beta_\nu = \kappa_\nu^g + \pi \int_0^\infty \chi_{e\nu}\left(m, \frac{2\pi r}{\lambda}\right) n(r) r^2\, dr \quad (24)$$

$$\omega_\nu = \frac{\pi \int_0^\infty \chi_{s\nu}\left(m, \frac{2\pi r}{\lambda}\right) n(r) r^2 dr}{\beta_\nu} \quad (25)$$

Turbulence Model

The following two-layer turbulence model is used to calculate eddy viscosity and eddy conductivity for fully-developed turbulent flow.

Inner Region

$$\varepsilon_m = 0.16\,(y+\Delta y)^2\,(1-\exp[-(y+\Delta y)/A])^2 \left|\frac{\partial u}{\partial y}\right| \quad (26)$$

$$\varepsilon_h = 0.176\, y(y+\Delta y)\,(1-\exp[-(y+\Delta y)/A])\,(1-\exp(-y/B))\left|\frac{\partial u}{\partial y}\right| \quad (27)$$

where the coefficients, A and B, depend on the pressure gradient,

$$A = 26\,\frac{\nu}{u_\tau}\left(\frac{\rho}{\rho_w}\right)^{1/2} \Big/ \left(1-11.8\,\frac{\nu_w u_c}{u_\tau^3}\,\frac{\rho_c}{\rho_w}\,\frac{du_c}{dx}\right)^{1/2} \quad (28)$$

and

$$B = \frac{35}{26} A \quad (29)$$

In Eqs. (26) and (27), Δy represents the coordinate displacement effect resulting from wall roughness, and is given as a function of the roughness Reynolds number, $k_s^+ \left(\equiv \frac{k_s u_\tau}{\nu_w}\right)$ as,

$$\Delta y = 0.9\,(\nu_w/u_\tau)\left[\sqrt{k_s^+} - k_s^+ \exp(-k_s^+/6)\right] \quad (30)$$

Outer Region

$$\varepsilon_m = 0.0168 \int_0^\delta (u_c - u)\, dy \quad (31)$$

$$\varepsilon_h = 0.0185 \int_0^\delta (u_c - u)\, dy \quad (32)$$

For smooth walls, the above turbulence model has been extensively tested by Cebeci and Smith[9] for flows with and without pressure gradients. For rough walls, the hydrodynamic part of the above model has been verified by Cebeci and Chang[10] for flows with adverse, zero, and favorable pressure gradients. The complete turbulence model, hydrodynamics, as well as heat transfer, has been

recently validated by Ahluwalia and Doss.[11]

Complete Numerical Solution

Before being finite-differenced, the gasdynamic equations are transformed into Von Mises stream function coordinates. The new coordinate system has the advantages of adjusting itself automatically to the height of the diffuser, of implicitly satisfying the continuity equation, and of reducing by one the number of equations to be solved, without raising the order of the equations. To ensure that the conservation equations are satisfied everywhere, the transformed equations are integrated over a control volume in the finite difference grid network. For accuracy, the dependent variables are assumed to vary quadratically between the grid points in both streamwise and cross-stream directions. The nonlinear terms are locally linearized and the resulting tri-diagonal form of algebraic equations easily inverted by using the Gauss elimination technique.

A unique feature of the numerical procedure is that no iterations are required for the specific purpose of calculating the pressure gradient. The details of the method of decomposition used to accomplish this may be found in Ref. 12. The radiation terms in the energy equation are treated as source terms, i.e., they are evaluated for a temperature distribution prevailing at the immediately preceding upstream station. Spectral integration involved in Eq. (7) is made accurate by dividing the large integration domain (200 cm^{-1} to 15,000 cm^{-1}) into 7 bands. Integration over these bands is performed by adopting a 16-point Gaussian quadrature scheme. As indicated in the previous paper,[1] radiation terms are not updated at each marching step, nor are they calculated at all grid points at any step. Had these modifications not been adopted, the computational time would have been on the order of 20 hours CPU time, as opposed to 15 to 30 minutes now typically required. Numerical computations were performed on IBM 370/195 and IBM 3033 machines.

Finally, the particle spectrum is input to the computer program in the form of histograms so that Eqs. (24) and (25) are numerically evaluated as follows:

$$\beta_\nu = \kappa_\nu^g + \pi \sum_i \chi_{e\nu}\left(m, \frac{2\pi r_i}{\chi}\right) \bar{N}_i \bar{r}_i^2 \qquad (33)$$

and

$$\omega_\nu = \frac{\pi \sum_i \chi_{s\nu}\left(m, \frac{2\pi r_i}{\lambda}\right) \bar{N}_i \bar{r}_i^2}{\beta_\nu} \qquad (34)$$

where K_ν^g is the absorption coefficient of the gas.

III. Results and Discussion

The exit conditions of the preceding work for the channel with rough walls (see Ref.1) are taken as the natural entrance conditions for the diffuser; these are: pressure = 0.85 atm, centerline temperature = 2350 K, and boundary layer thickness = 0.51 m. The mass flow rate through the diffuser is 350 kg/s. The diffuser is selected to be 15 m in length and, to be compatible with the channel of Ref. 1, measures 2m x 2m at inlet. The diffuser walls are considered to be moderately rough, of 3 mm roughness; as is characteristic for slag-coated walls, a wall temperature of 1800 K is assumed. The base calculations are performed for Rosebud coal ash, wall emissivity of 0.8 and diffuser divergence half-angle of 1.43 degrees. Sensitivity of the results to changes from base conditions is assessed by studying the diffuser behavior for Centralia power plant coal ash, for wall emissivity of 0.5, and for diffuser divergence half-angles of 1.0, 2.0, 2.5, and 3.0 degrees.

To be consistent with the channel calculations, thermodynamic properties corresponding to combustion of 5% moist coal with preheated, oxygen-vitiated air are used. For reasons explained in Ref. 1, mole fractions of CO_2, H_2O, and K are taken as 0.20, 0.12 and 0.004 in that order.

Histograms

As pointed out in the Introduction, slag particles play a dominant role in promoting radiative heat transfer in the diffuser. These slag particles originate mostly from the ash vaporized in the combustor and subsequently nucleated in the channel. Some of the unvaporized slag particles also flow into the channel. Reference 1 showed that the slag particles are not mono-sized but have a characteristic bi-modal spectrum. This particle size spectrum was found to depend intimately upon the channel operating conditions, ash carryover rate, and liquid droplet-to-slag vapor ratio at channel inlet. The last two parameters are principally functions of combustor flow configuration. An objective of the present task is to study the diffuser performance for the various spectra of particle sizes at channel exit that were presented in Ref. 1.

It is important to recognize that the complete particle spectrum must be considered in computing the radiative heat transfer by slag particles. To emphasize this point, reference is made to Eqs. (22) and (23), which indicate the efficiency factors for extinction and scattering to be functions of two parameters, namely, the complex refractive index and the nondimensional group, $\frac{2\pi r}{\lambda}$. Equations (24) and (25) further emphasize the dependence of the extinction coefficient and scattering albedo on the particle distribution function.

Intuitively, small particles ($\frac{2\pi r}{\lambda} \ll 1$) absorb more radiation than they scatter, intermediate-size particles ($\frac{2\pi r}{\lambda} \sim 1$) absorb and scatter radiation in comparable amounts, and particles of large size ($\frac{2\pi r}{\lambda} \gg 1$) are more effective in scattering radiation. Mie theory confirms the validity of this intuition. It is worth mentioning that a sample calculation of

Ref. 13 proved that a cloud of gas containing monodispersed particles has lower emissivity than if it had distributed-size particles of the same number density and the same average size. With this background, we seek an accurate representation of particle spectra presented in Ref. 1. A simple and accurate representation is in the form of a histogram.

Figure 1 is a nine-band histogram representa-

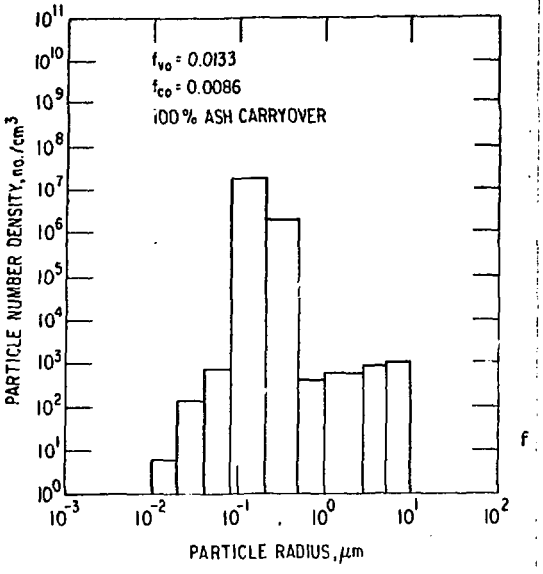

Fig. 1 Histogram for 100% Ash Carryover

tive of the particle size spectrum for 100% ash carryover into the channel. Figure 2 is an eight-

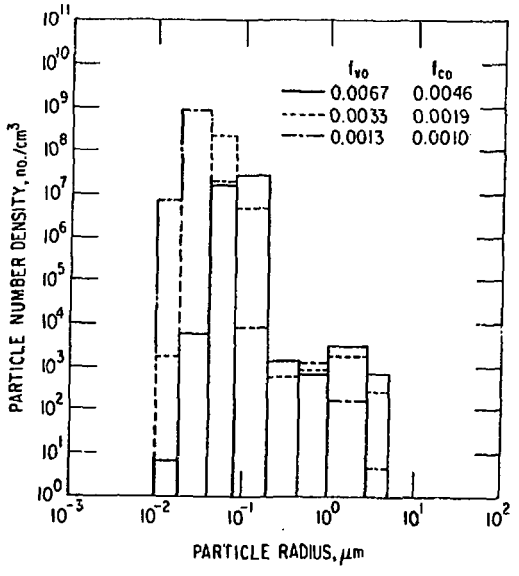

Fig. 2 Histogram for High Condensed Phase Carryover

band histogram for the situation in which the amount of ash vaporizing in combustor is less than the maximum possible. The histogram of Fig. 3

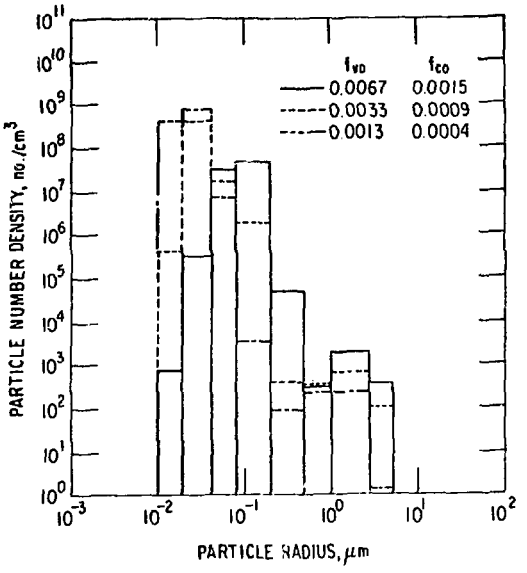

Fig. 3 Histogram for Low Condensed Phase Carryover

is for the case in which the vapor carryover rate into the channel is the same as in Fig. 2, but the condensed phase carryover rate is lower. Reference 1 should be consulted for detailed explanations concerning the spectra itself. In analogy to the concept of average size of a distribution function, the ordinates of these histograms were determined from the following equation:

$$\bar{N}_i = \frac{\Sigma N_j r_j}{\bar{r}_i} \qquad (35)$$

where i refers to a band, $\bar{r}_i$ is the median size of the band, and the summation is performed for all the particles lying within the band; $\bar{N}_i$'s calculated from Eq. (35) were used in determining β_ν and ω_ν in Eqs. (33) and (34).

Effect of Slag Carryover

Figure 4 shows the variation of radiative and convective heat flux along the diffuser length for particle spectra corresponding to the histograms of Fig. 2. The axial drop in convective heat flux is readily attributed to boundary layer growth. It is seen that the radiative heat flux increases along the axial direction. This increase is partly credited to divergent diffuser geometry, which leads to higher optical thickness downstream. More importantly, as flow Mach number decreases, a conversion of kinetic energy to thermal energy takes place. This conversion of energy more than compensates for the diffuser heat loss in the form of convection and radiation. Consequently, the centerline temperature, and the average temperature as

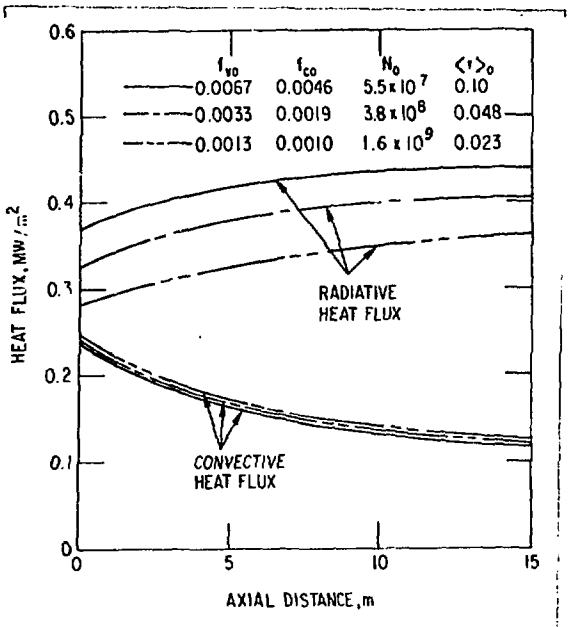

Fig. 4 Heat Flux Characteristics for *High Condensed Phase Carryover*

well, increase along the flow direction. This temperature rise is mainly responsible for increasing radiative heat flux along the flow direction. It is appropriate to point out here that the radiative heat flux for black body is proportional to the fourth power of temperature. The gas emissivity, however, decreases with temperature, so that the dependence of gas radiation on temperature is less than the fourth power. The radiation characteristic of slag particles-laden gas can depart from this general rule. The reason is that the electrical condcutivity of slag particles, a parameter that determines absorptivity, is exponentially dependent upon gas temperature. Therefore, depending on electrical conductivity variation and size and number density of particles, the exponent of temperature for proportionality between radiation of a gas medium containing slag particles and temperature may be greater than four.

Figure 4 dhows that radiative heat flux increases with the vapor carryover rate into the channel. There are two reasons for this. First, with a higher vapor carryover rate, in spite of lower number density, the particles have a greater collective surface area ($\pi\Sigma\bar{N}_i\bar{r}_i^2$), and this leads to a higher absorption coefficient. Secondly, with a higher vapor carryover rate, the number of particles in the larger size range increases (see Fig. 2). As mentioned earlier, larger particles ($\frac{2\pi r}{\lambda} >> 1$) scatter more radiation than they absorb, thus providing the smaller particles, which are effective absorbers, with an additional opportunity to absorb the scattered radiation. This process becomes more effective with the possibility of multiple scattering.

The importance of radiation in Fig. 4 is very pronounced. Radiative heat flux exceeds the convective flux by a factor as high as four. Figure 5 presents the results for histograms of Fig. 3.

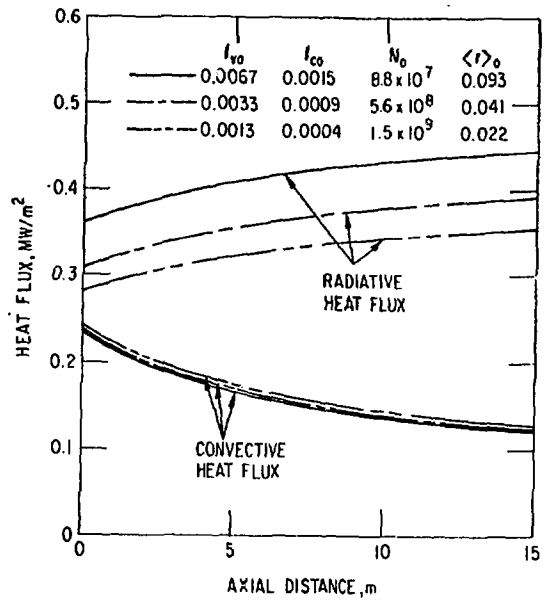

Fig. 5 Heat Flux Characteristics for Low Condensed Phase Carryover

In general, these results support the findings and discussion given for Fig. 4. The contribution of radiation can be directly ascertained from Fig. 6.

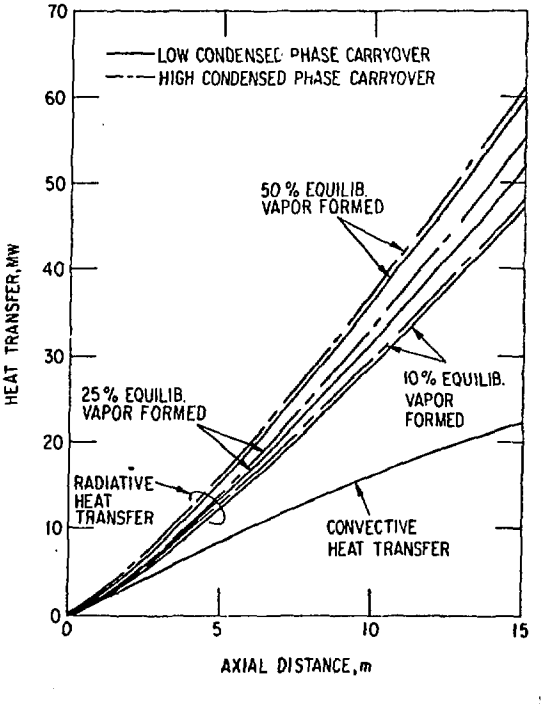

Fig. 6 Heat Transfer Characteristics

The heat transfer by convection is nearly 25 MW; the radiative heat transfer varies from 44 MW for

the case of 10% of equilibrium value of vapor formed in the combustor to 62 MW for the 50% case. For 100% ash carryover, the heat transfer by radiation is 79 MW (see Fig. 7). Figure 7 shows

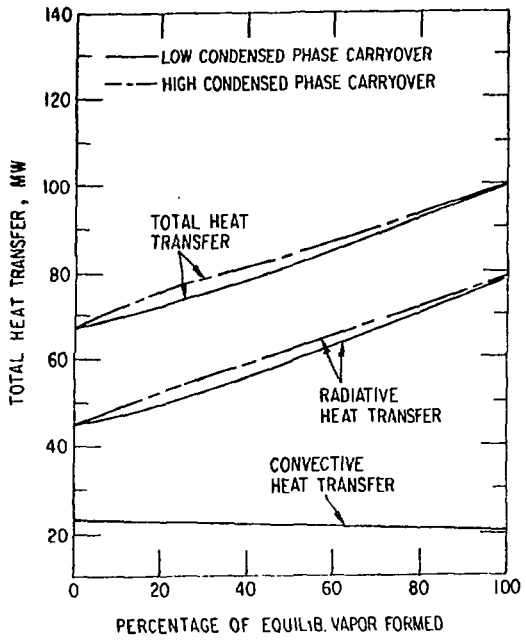

Fig. 7 Relationship Between Heat Transfer and Ash Carryover Rate

that results are more sensitive to the total ash carryover than to the individual fractions of vapor and condensed phases entering the channel. For all cases considered, the total heat transfer lies between 70 and 100 MW.

Sensitivity of Results

To identify the critical parameters that control heat transfer in the diffuser, results are given in Figs. 8, 9, and 10 by changing one or more conditions of the reference case. Curve A of Fig. 8 represents the base case. Note that radiative flux first increases and then decreases. At the front end of the diffuser, specific volume is small enough that the conversion of kinetic to thermal energy can compensate for the heat loss, so that there is a rise in temperature. Consequently, the radiative heat flux increases in magnitude. At the back end, because of divergent geometry, the reverse happens.

Curve B is for a hypothetical situation in which no potassium atoms are present. Curve C is for 23% ash carryover. In curve D, no particles are present; this would happen, for example, in a gas- or oil-fired MHD plant, except that mole fraction of water vapor would be much higher. Curve E represents the hypothetical situation in which neither particles nor potassium atoms are present. Curve F represents the contribution of convection.

The difference between curves A and C is attributed to the different particle spectra that

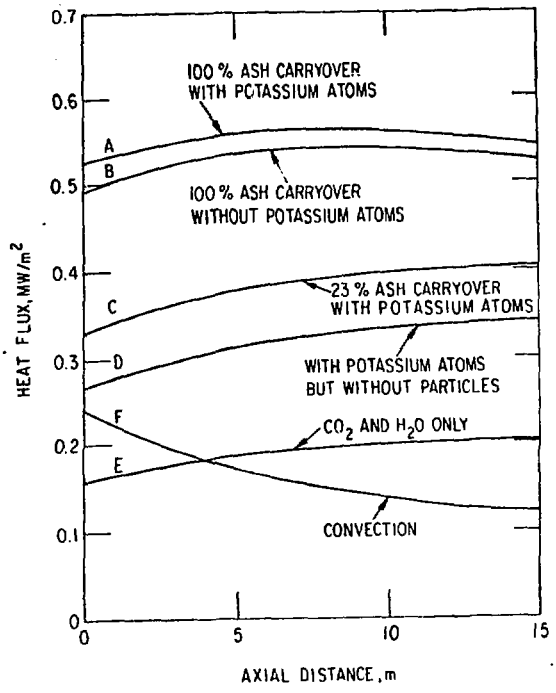

Fig. 8 Sensitivity of Results

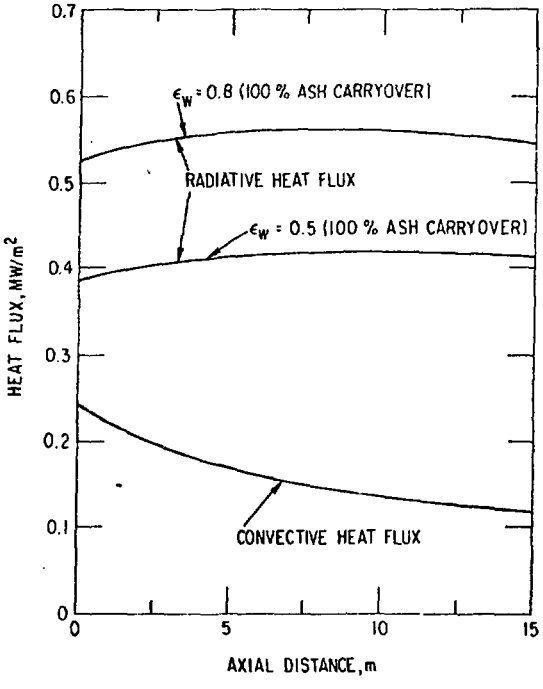

Fig. 9 Effect of Wall Emissivity on Heat Flux

result from change in the rate of ash carryover

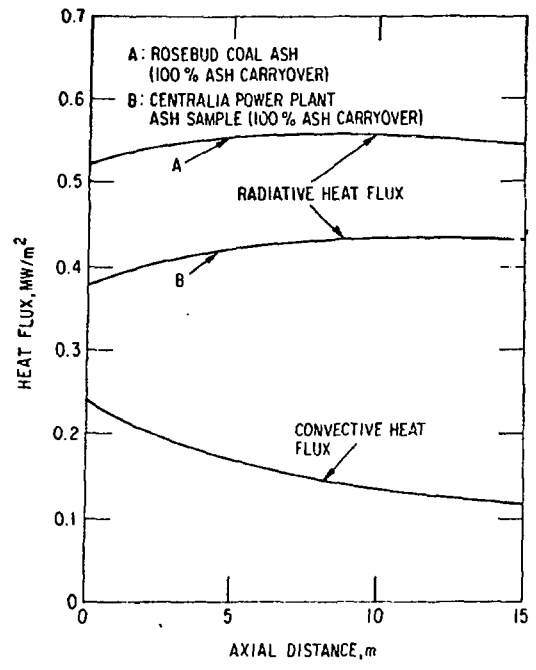

Fig. 10 Effect of Electrical Conductivity on Heat Flux

into the channel. The difference between curves A and D is a measure of the important role of the slag particles in promoting radiation. It is seen that the particle contribution is nearly 30 to 50% of the total radiative heat transfer. The difference between curves A and B measures the contribution of potassium atoms for the gas-plus-particles case, and between D and E indicates the contribution of K for the gas-only case. The differences between A and B and between D and E are not the same, thus proving the non-additive nature of contributions by individual participating species. It is interesting to note that particles tend to scatter the short wavelength radiation emitted by potassium. The disparity between the differences of curves A and B and of curves D and E is a measure of the radiation shielding effect of the particles by multiple scattering.

Figure 9 shows the influence of wall emissivity on radiation heat transfer. A 30% reduction of heat flux is observed when the wall emissivity is lowered to 0.5 from 0.8. A wall emissivity of 0.5 is believed to be the lower limit.

Figure 10 shows the effect of electrical conductivity of particles on radiative heat transfer. The electrical conductivity data of Refs. 14 and 15 have been curve-fitted by the following correlations:

Rosebud coal: $\sigma_e = 10 \exp (12.65-2.3\times10^4/T)$

Centralia: $\sigma_e = 0.5 \exp (13.5-2.08\times10^4/T)$

Electrical conductivity enters the calculations through complex refractive index ($\equiv 1.5-i30\lambda\sigma_e$). The higher the electrical conductivity of slag particles, the greater is the efficiency factor for extinction. Figure 10 indicates a 30% difference in radiation heat fluxes for Rosebud coal ash, considered to be of medium electrical conductivity, and Centralia power plant coal ash,[15] considered to be of low electrical conductivity.

Diffuser Performance

Figure 11 presents the influence of diffuser

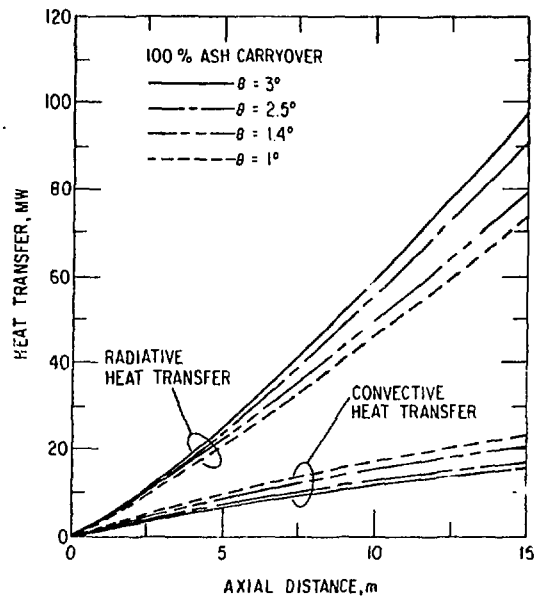

Fig. 11 Diffuser Performance

half-divergence angle on heat transfer. The greater the divergence angle, the higher the specific volume and more is the radiative heat flux. The lowering of convective heat flux with divergence angle is indicative of greater rate of boundary layer growth. In Table 2, the average velocity and blockage at diffuser exit, and the corresponding pressure recovery coefficient, are listed. For 3° divergence angle, the flow may separate anywhere beyond x = 10 m. For all four cases, the average exit temperature was ~2300 K. For 2.5° and 3.0° divergence angles, the flow became fully developed before reaching the exit.

Table 1. Diffuser Performance

θ	Area Ratio	< u > m/s	Blockage	Cp	Comment
1.0	1.58	453	0.45	0.33	No boundary layer separation
1.4	1.87	406	0.54	0.39	No boundary layer separation
2.5	2.71	317	0.66	0.46	Fully developed flow
3.0	3.17	283	0.69	0.48	Separation tendency

IV. Significant Impacts of Results

1. System Design

Heat flux to channel and diffuser walls influences selection of wall material and design of the wall-cooling system, and may dictate certain system design considerations for the bottoming plant. To elaborate upon the impact of heat flux on the system design considerations, a back-of-the-envelope calculation has been done. In one of the several system design configurations proposed for the bottoming steam plant, feedwater from the condenser is pumped to the economizer and then passes to the walls of the combustor, MHD channel, and diffuser. Thereafter, the feedwater flows into a steam holding drum. From the steam drum, a part of the feedwater is drained from the bottom, passed to the wall of the radiant boiler, and returned to the holding drum. Saturated steam is drawn from the top of the drum to flow into a superheater.

It is expected that half the total electrical power will be generated by the MHD topping cycle and the other half by the steam bottoming cycle. Therefore, to obtain a rough estimate of temperature rise of feedwater through the power train components (combustor, nozzle, channel, and diffuser), assume that, for the channel generating 285 MW_e, (see Ref. 1) (the diffuser configuration of the present work complements the exit conditions of this channel), the bottoming plant has a capacity of 300 MW_e. For a specific steam flow rate of 5.32 lbs/kWh through the turbine -- typical of a 813 K/813 K/23.7 MPa supercritical single reheat steam cycle -- the required water flow rate is 200 kg/s. A conservative estimate of feedwater temperature rise through the power train can be made by assuming that all the feedwater flows sequentially through the combustor, nozzle, channel, and diffuser. A simple heat balance calculation can be performed by assuming the state conditions of feedwater at the exit of the economizer; allowing for pressure drop, a reasonably accurate state condition may be 373 K/30 MPa.[16]

Depending upon the combustor flow configuration, a heat loss (mainly by radiation) equivalent to 5% of total thermal input to the combustor may be incurred across the combustor and nozzle walls. This translates into 85 MW heat transfer to feedwater for the channel operating conditions being considered. The feedwater temperature rises to 495 K in response to 85 MW of heat transfer. Reference 1 calculated a heat transfer of 61 MW by radiation and 89 MW by convection across the rough channel walls. This 150 MW of heat transfer results in elevating the feedwater temperature to 650 K.

The present study has revealed conclusively that the heat transfer in the diffuser depends, among other things, on the rate of ash carryover into the channel. For entrance conditions complementing the channel exit conditions of Ref. 1, Fig. 7 shows a radiative heat transfer (by gas and particles) of 79 MW and a convective heat transfer of 21 MW to occur in the diffuser for 100% ash carryover into the channel. With 100 MW of heat transfer, heat balance indicates that the feedwater will boil on its passage through the diffuser wall; the temperature at diffuser exit will be 740 K if a feedwater pressure drop of 3 MPa is assumed to occur while flowing from the economizer to diffuser exit. For ease of comprehension, the various state points in the feedwater flow circuit are shown in Fig. 9. The first and foremost conclusion is that the feedwater flow design of Fig. 12 may be inappropriate from the viewpoint of

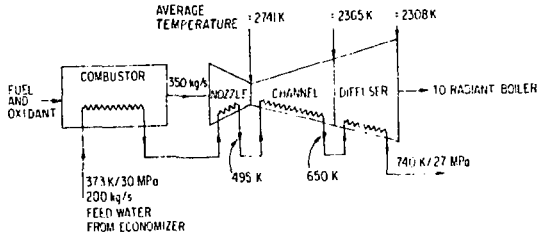

Fig. 12 Simplified Feedwater Flow Diagram

designing the diffuser wall-cooling system. Clearly, ignoring the radiative contribution to heat transfer in performing channel and diffuser calculations, would result in an entirely misleading conclusion. Also, if the channel is scaled-up from the reference size (i.e., 285 MW_e), the above conclusion regarding system design remains equally valid. The reason is that the optical beam length, and, hence, the radiative heat transfer scale-up with channel size.

2. NO_x Problem

We have seen that the large heat transfer rates in the MHD channel and diffuser, resulting, in part, from enhancement by gas radiation in the channel and by gas-plus-particles radiation in the diffuser, may cause the feedwater to boil in the diffuser. Therefore, for the purpose of system design analysis, it is more appropriate to regard the diffuser as a part of the radiant boiler. It is generally believed that NO_x can be decomposed if the average temperature of the combustion products leaving the diffuser is higher than 2200 K.[17] Despite the

radiation enhancement, the average temperature is found to be 2300 K, so that, as far as NO_x decomposition is concerned, the radiation enhancement does not add significantly to the problem.

Previous to the accurate heat transfer calculations presented in this work, designing a radiant boiler required consideration of two mutually conflicting effects. The heat transfer rate in the boiler had to be mitigated in order to maintain the gas at a high temperature long enough that NO_x could be decomposed. Yet, the heat transfer rate had to be sufficient to boil the feedwater. Because the present calculations indicate that the boiling will take place in the diffuser itself, a large amount of heat extraction in the radiant boiler appears to be unnecessary. Consequently, if required, the refractory walls of the radiant boiler can be made as thick as desired.

V. Conclusions

A quasi-three-dimensional diffuser model has been formulated and solved by an analytical-cum-numerical technique. The radiative contributions of carbon dioxide, water vapor, and potassium atoms are all included. The formulation also incorporates the role of slag particles in absorbing and scattering radiation. The important conclusions that can be drawn from the results of the analysis are listed below.

1. Although the convective heat flux in the diffuser decreases along the axial direction (because of boundary layer growth), the radiative heat flux may increase in that direction because of diffuser divergence and possible rise in temperature resulting from the conversion of kinetic to thermal energy. For the base conditions, the total convective heat transfer in the diffuser is 25 MW, and the radiative heat transfer lies between 44 MW for 8% ash carryover and 79 MW for 100% ash carryover into the channel. This shows the importance of accounting for radiation in diffuser heat transfer computations.

2. The results demonstrate that the slag particles play a dominant role in promoting radiation. Comparing the curves B and E of Fig. 8, it can be inferred that the radiative flux resulting from particles is more than twice that resulting from carbon dioxide and water vapor. The results of Fig. 8 also highlight the radiation shielding effect of the particles through multiple scattering. This shielding effect is a manifestation of the particles scattering the short wavelength radiation that is emitted by potassium.

3. The sensitivity of results to changes from reference conditions has been established. It was observed that changing the wall emissivity from 0.8 to 0.5, or changing the electrical conductivity, modifies the radiative flux by 30%. The influence of diffuser half-divergence angle on heat transfer has been discussed. In view of the importance of radiation, the influence of various operating parameters on diffuser performance, as studied in Ref. 2 with radiation omitted, needs further elaboration.

4. The impact of heat transfer enhancement by gas radiation in the channel and by gas-plus-particles radiation in diffuser on system design has been evaluated. A crude, but conservative estimate reveals that the feedwater will boil in the diffuser itself, before reaching the radiant boiler. Therefore, from the system design point of view, it is more logical to regard the diffuser as a part of the radiant boiler.

5. Despite the radiation enhancement in heat transfer, the gas temperature at the diffuser exit is much higher than 2200 K, so that no formidable difficulty in decomposing NO_x is anticipated. Moreover, because the feedwater boils in the diffuser, the requirement of maintaining a heat transfer high enough to boil feedwater in the radiant boiler is relieved. Consequently, the heat transfer rate in the radiant boiler can be mitigated (for example, by thickening boiler walls) to as small a level as desired in order to maintain the gas at an adequately high temperature. This provision is likely to simplify the design procedure for an MHD radiant boiler -- which should, perhaps, now be more appropriately referred to as the NO_x decomposition chamber.

Acknowledgements

This research was sponsored by DOE/MHD Division. The authors greatly appreciate the help of their colleague, Dr. G. Berry, in resolving the issues relating to the impact of radiation enhancement in heat transfer on system design.

References

1. Im, K. H., and Ahluwalia, R. K., "*Heat Transfer Including Radiation and Slag Particles Evolution in MHD Channel-I*," AIAA 18th Aerospace Science Meeting, Pasadena, CA, Jan. 1980, AIAA Paper No. 80-0250.

2. Doss, E. D., "*Subsonic MHD-Diffuser Performance with High Blockage*," Journal of Energy, Vol. 1, 1977, p. 370-375.

3. Roy, G. D., "*On Supersonic and Subsonic Diffusers for Magnetohydrodynamic Generator Applications*," Fluids Engineering in Advanced Energy Systems, Conference Proceedings of the Winter Annual Meeting of ASME, Dec. 1978, p. 139-152.

4. Van De Hulst, H. C., Light Scattering by Small Particles, John Wiley & Sons, Inc., New York, 1979, p. 119-128.

5. Tien, C.L., "*Thermal Radiation Properties of Gases*," Advances in Heat TRansfer, Vol. 5, 1968, p. 253-324.

6. Petrick, M. and Shumyasky, B. Ya., Open-Cycle Magnetohydrodynamic Electrical Power Generation, A Joint U.S.A./U.S.S.R. Publication, Argonne National Laboratory, Argonne, IL, 1978, p. 622-676.

7. Davis, P. and Sykes, J. B., Neutron Transport Theory, Chapter XII, Oxford University Press, Amen House, London, 1958, p. 157-173.

8. Mark, C., "*The Spherical Harmonic Method I*," National Research Council of Canada, Division of Atomic Energy, TM-92, 1944.

9. Cebeci, T. and Smith, A.M.O., Analysis of Turbulent Boundary Layers, Chapter 6, Academic Press, New York, 1974.

10. Cebeci, T. and Chang, K. C., "*Calculation of Rough-Wall Boundary-Layer Flow,*" AIAA Journal, Vol. 16, No. 6, 1971, p. 993-1003.

11. Ahluwalia, R. K. and Doss, E. D., "*Convective Heat TRansfer in MHD Channels and its Influence on Channel Performance,*" AIAA 18th Aerospace Science Meeting, Pasadena, CA, Jan. 1980, AIAA Paper No. 80-0178.

12. Ahluwalia, R. K. and Doss, E. D., "*Simulation of Three-Dimensional MHD Duct Flow,*" Presented at National Conference on Numerical Methods in Heat Transfer held at College Park, MD, Sept. 1979.

13. Im, K. H. and Johnson, R., "*Effective Emissivity and Absorptivity of Combustion Gas with Slag Particles,*" Argonne National Laboratory, ANL/MHD-79-14, to be published.

14. Pallina, R. and Larsen, R., "*MHD Slag Conductivity Studies,*" 17th Symposium on Engineering Aspects of MHD, Stanford, CA, March 1978, p. C.6.1-C.6.6.

15. Petrick, M. and Shumyasky, B. Ya, Open-Cycle Magnetohydrodynamic Electrical Power Generation, Chapter 13, A Joint U.S.A./U.S.S.R. Publication, Argonne National Laboratory, Argonne, IL 1978, p. 559-568.

16. Berry, G., Private Communication, Argonne National Laboratory, Argonne, IL

17. Sistino, A. J., "*Analytical Studies of NO_x Decomposition in the Radiant Boiler of an Open-Cycle MHD Power Plant,*" Argonne National Laboratory, ANL/MHD-79-7, April, 1979.